JGR Atmospheres

RESEARCH ARTICLE
10.1029/2018JD028957

# Three-Year Continuous Observation of Pure and Polluted Dust Aerosols Over Northwest China Using the Ground-Based Lidar and Sun Photometer Data

**Z. Zhang[1,2], J. Huang[1,2], B. Chen[1,2], Y. Yi[3], J. Liu[4], J. Bi[1,2], T. Zhou[1,2], Z. Huang[1,2], and S. Chen[1,2]**

[1]College of Atmospheric Sciences, Lanzhou University, Lanzhou, China, [2]Key Laboratory for Semi-Arid Climate Change of the Ministry of Education, Lanzhou, China, [3]College of Earth environment Sciences, Lanzhou University, Lanzhou, China, [4]School of Mechanical and Instrument Engineering, Xi'an University of Technology, Xi'an, China

**Key Points:**
- The results were based on three years of continuous ground-based lidar and sun photometer data simultaneously observed at SACOL
- The peak value of the volume depolarization ratio was 0.21 and 0.31 for pure dust and polluted dust, respectively, and the threshold value was 0.25
- The distributions of volume depolarization ratio and color ratio for pure dust aerosols was wider than that for polluted dust, and a positive correlation between them was observed

**Correspondence to:**
J. Huang,
hjp@lzu.edu.cn

**Citation:**
Zhang, Z., Huang, J., Chen, B., Yi, Y., Liu, J., Bi, J., et al. (2019). Three-year continuous observation of pure and polluted dust aerosols over Northwest China using the ground-based lidar and sun photometer data. *Journal of Geophysical Research: Atmospheres*, *124*. https://doi.org/10.1029/2018JD028957

Received 6 MAY 2018
Accepted 29 DEC 2018
Accepted article online 7 JAN 2019



**Abstract** Mineral dust is a dominant aerosol type in northwestern China and can mix with other air pollutants during its long-range transport, playing an important role in Earth's energy budget and hydrological cycle on both regional and global scales. In this study, the optical properties of pure dust and polluted dust were compared by using ground-based lidar and sun photometer data at SACOL (Semi-Arid Climate and Environment Observatory of Lanzhou University) from August 2009 to August 2012. The total attenuated backscattering coefficient at 532 nm, the volume depolarization ratio (VDR) and the color ratio (CR) derived from the L2S-SM-II dual-band polarization lidar and aerosol optical depth (AOD) and Angstrom exponent from sun photometer data were used to identify pure dust and polluted dust. The results showed that AOD at 440 nm of pure dust was widely distributed within the range of 0.4–1.1 but the AOD of polluted dust was generally less than 0.6. The frequency distribution of VDR showed that the mean value of pure dust was greater than that of polluted dust and the peak values were 0.31 and 0.21, respectively. The frequency distribution of CR showed that the mean value of pure dust was larger than that of polluted dust, and it was mostly pure dust aerosol when color ratio was greater than 0.8. The VDR showed a positive correlation with CR. Using the frequency distribution of VDR, a threshold value of 0.25 was proposed to differentiate pure dust from polluted dust. The rates of misclassification were 20.7% and 18.6% for pure dust and polluted dust, respectively. This work will be helpful for the classification of aerosol types in satellite observations and numerical modeling.

## 1. Introduction

Mineral dust is one of the most important types of tropospheric aerosols (Huang et al., 2014) and can affect the Earth-atmosphere's radiation budget by absorbing and scattering solar/terrestrial radiation (direct effect; Huang et al., 2009; Li, 2004; Shi et al., 2005; Sokolik & Toon, 1996), alter the optical properties and lifetime of clouds (indirect effect; e.g., Sassen, 2002), and enhance the evaporation of cloud droplets, further reduce the cloud water path of warming clouds (semdirect effect; Huang, Lin, et al., 2006), all of which can impact the climate system (Huang et al., 2005; Huang, Lin, et al., 2006; Huang, Minnis, et al., 2006; Twomey et al., 1984), especially in semiarid regions over East Asia (J. Huang et al., 2010; Huang et al., 2014). Dust can also change the global climate by serving as ice nuclei and changing cloud properties (Xie et al., 2013). Dust aerosols have obvious heating or cooling effects that can change the atmospheric thermal circulations and dynamics (Kang et al., 2017). However, the existing atmospheric dust loading cannot be explained by natural sources alone, and anthropogenic dust is also a contributing factor (Tegen & Fung, 1995). The atmospheric dust that originates from soils disturbed by human activities, such as land use practices, can be interpreted as *anthropogenic* dust (Huang et al., 2015; Tegen & Fung, 1995).

Local anthropogenic dust aerosols associated with agricultural and industrial activities account for 25% of the total dust burden in the atmosphere (Huang et al., 2015). More than 53% of the anthropogenic dusts come from semiarid and semiwet regions (Guan et al., 2016). These anthropogenic dusts can increase atmospheric dust loading, which in turn induces radiative forcing (Chen et al., 2017, 2018; Tegen & Fung, 1995). The annual average anthropogenic dust column burden values range from 0.42 g/m$^2$ maximum in India to 0.12 g/m$^2$ minimum in North America (Huang et al., 2015). Previous works (Guan et al., 2016) have also explored the relationship between anthropogenic dusts and population over semiarid regions on a global scale. The results show that a positive correlation between anthropogenic dust and population is

more obvious for croplands than for other land cover types (crop mosaics, grassland, and urbanized regions). The most significant relationship between anthropogenic dust and population was found in the semiarid region of India, where is a high portion of croplands.

Although there are some quantitative assessments about the anthropogenic dust loading, the accuracy of these results is still under investigation due to the limitation of data sets and detection methods. In Huang's method (Huang et al., 2015), approximately 9.6% of the anthropogenic dust is misclassified as natural dust and 8.7% of the natural dust is misclassified as anthropogenic dust within the planetary boundary layer. East Asia has the highest concentration of anthropogenic aerosols in the world (Sugimoto, Nishizawa, Shimizu, Matsui, Jin, et al., 2015). It is also a unique region where mineral dust sources are located near urban and industrial areas. During transport, dust often mixes with anthropogenic aerosols, producing polluted dust, which induces more serious environmental and climatic problems (Su et al., 2008).

Asian advanced active remote sensing instrument with high resolution and accurate detection abilities in the lower altitudes, lidar has become an important approach to detecting the spatial and temporal distributions of aerosol properties (Zhou, Huang, Huang, Li, et al., 2013; Zhou, Huang, Huang, Liu, et al., 2013). Hua and Kobayashi (2005a, 2005b) and Hua et al. (2005a, 2005b, 2007) used ultraviolet Rayleigh-Mie lidar and Raman lidar for detecting the temperature profile in the troposphere. Chen et al. (2010) and Liu et al. (2014) used the satellite-based Cloud-Aerosol lidar with Orthogonal Polarization to detect the dust layers with fewer misclassifications. Zhao et al. (2014) used the micropulse lidar to detect aerosols and clouds, and Wang et al. (2018) used the ceilometer to develop methods for cloud base detection. However, ground-based lidar has an obvious advantage over satellite-based lidar when detecting dust particles near the surface. In the present study, the ground-based lidar measurements were used to validate the thresholds used in the detection method of anthropogenic dust (Huang et al., 2015).

The paper is arranged as follows. The details of the data sets are given in section 2. In section 3, the inversion and detection method is introduced. Examples of distinguishing pure dust and polluted dust are presented in section 4. A comparison of the optical properties of two dust cases is presented in section 5. The conclusion and discussion are presented in section 6.

## 2. Data and HYSPLIT Model

### 2.1. Surface Station Data

The global surface weather data set (http://www.cma.gov.cn/2011qxfw/2011qsjgx/) from the China Meteorological Administration State Information Center was used in this study. This data set is derived from the surface hourly data on the global scale and which were decoded and normalized. The temporal coverage of the data set spans from 1 January 1980 to 1 June 2015. The data set is strictly quality controlled. Here we analyzed the present-time weather phenomena at Yuzhong station from August 2009 to August 2012. Figure 1 shows the spatial distribution of dust events from October 2009 to June 2013 in China, with colors representing the number of dust event. The location of SACOL (Semi-Arid Climate and Environment Observatory of Lanzhou University) is shown in green, and the nearby dust source includes Taklimakan Desert and the Gobi Desert. Dust events occur mainly in the arid and semiarid areas. It can be seen from Figure 1 that most dust weather occurred in northern China with the frequent dust days occurred over the two source regions, that is, the Gobi Desert in Inner Mongolia along the Northern China, and the surrounding areas of the Taklamakan Desert in Xinjiang. The total dust days was about 10 in most northern China and over 80 in most source regions. The dust days around the SACOL site was in the medium, varied from 10 to 50.

### 2.2. Lidar and Sun Photometer Measurements

L2S-SM-II dual-band depolarization lidar from the National Institute for Environment Studies (NIES) and the Cimel Electronique sun photometer (CE-318) are operated at SACOL and have observed aerosols and clouds since August 2009 (Huang et al., 2008; Liu et al., 2011). NIES lidar and sun photometer data at SACOL were part of Asian Dust Network and Aerosol Robotic NETwork, respectively. SACOL is situated on the Loess Plateau (35.946°N, 104.137°E) at approximately 1,965.8-m above sea level. The topography of SACOL is characterized by plains, ridges, and mounds, etc. Its surrounding area is flat and covered with

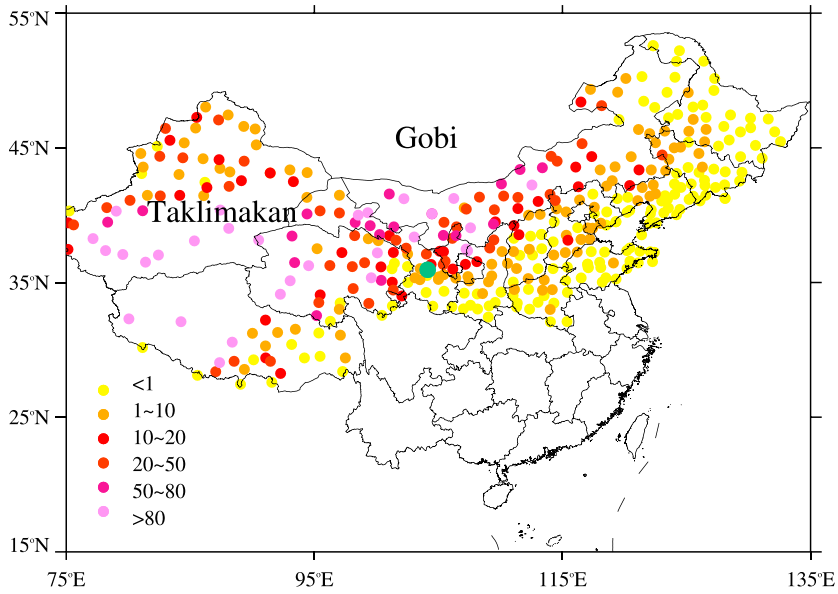


**Figure 1.** Spatial distribution of dust events in China. Colors represent the number of dust events. The location of Semi-Arid Climate and Environment Observatory of Lanzhou University is shown in green. The nearby dust source (Taklimakan desert, Gobi desert) is also shown.

short grass. The site was built on the top of Cuiying Mountain because the environment here is rarely affected by human activity. Thus, the climate at the site can represent that of the surrounding hundreds of kilometers.

The L2S-SM-II dual-band depolarization lidar is a two-wavelength polarization-sensitive backscatter lidar, and its structure is shown in Figure 2. This lidar system consists of three parts: the laser source, signal receipt system, and data recording device. The temporal and vertical resolution of the lidar structure is 15 min and 6 m, respectively. The so-called linear iterative method (Elterman, 1966) and the Fernald method (Fernald, 1984) were most widely used for deriving particulate extinction and backscatter coefficients from calibrated, range-corrected lidar signals. In this study, all sky data were used. In our procedure, first cloud base was detected, and data higher than this height are eliminated. Thus, the cloud does not effect on the aerosol retrieval. Next, vertical profile of S/N ratio is checked and the analysis range is limited to good S/N region (height section). If there was optically thick layer near the ground, S/N in middle troposphere becomes worse and upper limit of inversion decreases. Thus, we can assume the accuracy is almost uniform in the region where extinction coefficient was calculated.

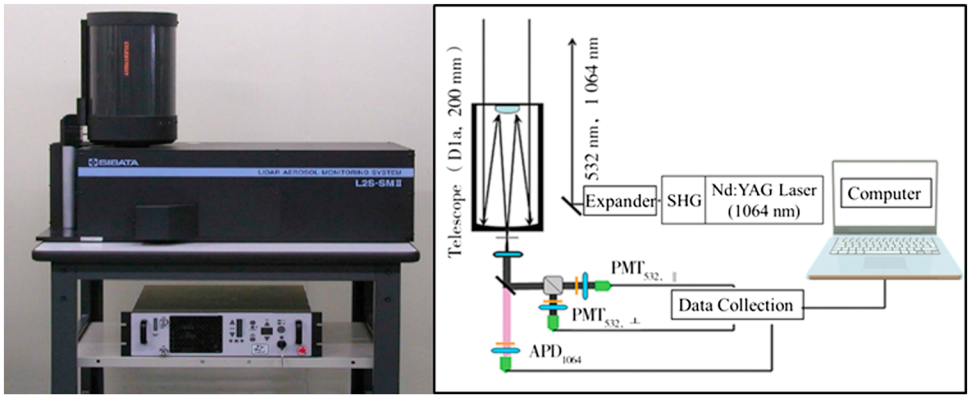


**Figure 2.** The structure of L2S-SM-II dual-band depolarization lidar at Semi-Arid Climate and Environment Observatory of Lanzhou University.

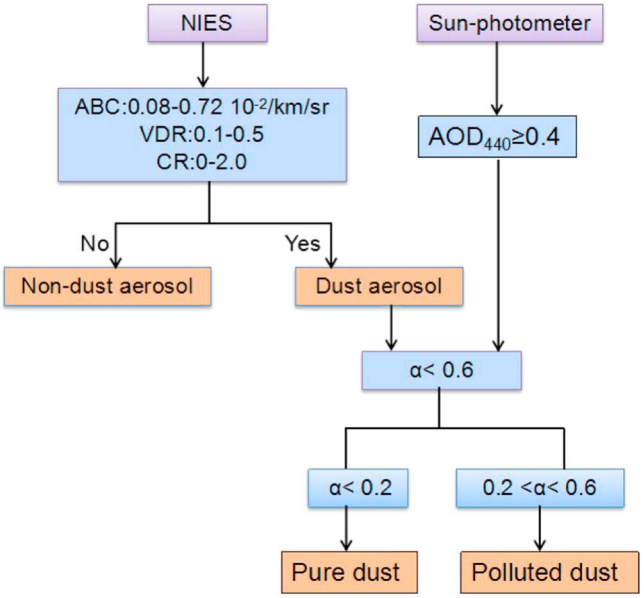


**Figure 3.** Flow chart of dust detection method. NIES = ; AOD = aerosol optical depth; VDR = volume depolarization ratio; ABC = attenuated backscattering coefficient; CR = color ratio.

Here vertical profiles of the aerosol optical properties were derived using the Fernald method (Zhou, Huang, Huang, Liu, et al., 2013; Zhou, Huang, Huang, Li, et al., 2013). The total attenuated backscattering coefficient (ABC) at 532 nm, the volume depolarization ratio (VDR), and the color ratio (CR) were derived. The CE-318 takes measurements of direct solar irradiances at multiple discrete channels within the spectral range of 340–1640 nm, which can be used to calculate aerosol optical depth (AOD), Angstrom component (AC) and fine-mode fraction. In this study, we examined a continuous period from August 2009 to August 2012.

### 2.3. Satellite Data Sets

The OMI (Ozone Monitoring Instrument) is on board Aura, a member of the A-Train satellite constellation. OMI mainly observes ozone and other key air quality molecules such as $NO_2$, $SO_2$, BrO, OClO, and aerosol. OMI data sets can be distinguished among different aerosol types, such as smoke, dust, and sulfates. The aerosol index (AI) is provided in OMI level 3 daily aerosol gridded products, representing a good indicator for absorbing aerosols including dust aerosols. CALIPSO (Cloud-Aerosol Lidar and Infrared Pathfinder Satellite Observation) is also a member of A-Train satellite constellation. This satellite provides a new insight into the role of clouds and aerosols in regulating Earth's weather, climate, and air quality. Vertical distribution of aerosol type along the orbit is provided by the CALIPSO level 2 VFM product.

### 2.4. HYSPLIT-4 Model

The HYSPLIT-4 (fourth-generation Hybrid Single-Particle Lagrangian Integrated Trajectory) transport model provided by the National Oceanic and Atmospheric Administration Air Resources Laboratory was used to calculate the simple air-parcel trajectories with interpolated meteorological fields. Back trajectory simulation produced with the HYSPLIT-4 model was used to explore the most likely sources and transportation path of the dusts. The 6-hr-interval final archive data were generated from the National Centers for Environmental Prediction Global Data Assimilation System reanalysis three-dimensional meteorological fields. The spatial and time resolution was 1° and 6 hr, respectively. The start time for simulation was 19 March 2010 and 29 July 2010. The simulation time was 36 and 18 hr, respectively.

## 3. Detection Methods

Lidar and sun photometer data were both used to discriminate pure dust and polluted dust aerosols. The flowchart of the detection method used here is shown in Figure 3.

### 3.1. Dust Detection by a Depolarization Lidar

Generally, cloud droplets have a larger ABC and higher CR (~1) values than aerosol particles. However, mineral dust and marine aerosol have a relatively large CR value under higher relative humidity conditions. These scattering features can be used to distinguish aerosols from clouds (Zhao et al., 2014). The attenuated backscattering coefficient is vital in many aspects. Accurate aerosol and cloud heights and the retrieval of extinction coefficient profiles are all derived from the total backscatter measurements (Garrett & Zhao, 2013; Wang et al., 2018; Zhao et al., 2012, 2014, 2016). Additionally, the VDR is a useful indicator to identify nonspherical particles and provides an opportunity to discriminate dust aerosols.

The classical lidar equation is expressed as follows,

$$P(z)\cdot z^2 = E\cdot C\cdot \beta(z)\cdot T^2(z),$$

where $P(z)$ is the return signal that is proportional to the received power from a scattering volume at slant range $z$; $E$ is an output energy monitor pulse, which is proportional to the transmitted energy; $C$ is the calibration constant of the instrument, which includes losses in the transmitting and receiving optics and the

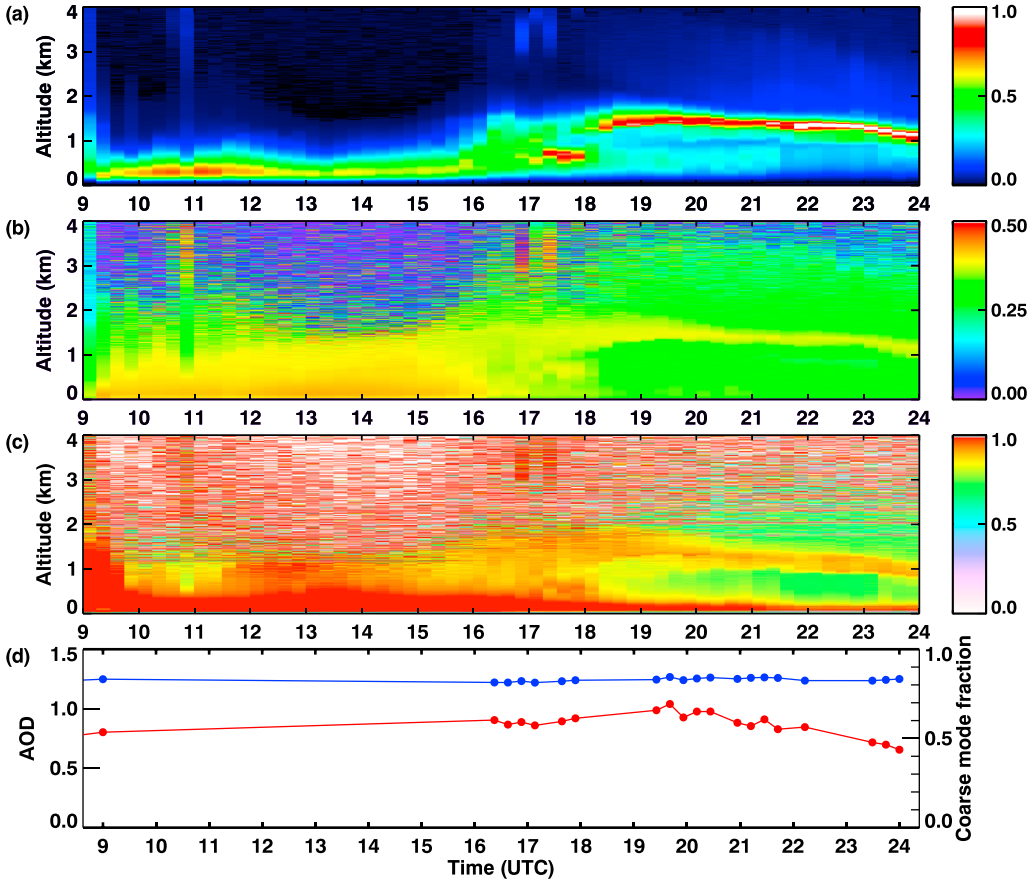


**Figure 4.** Distribution of attenuated backscattering coefficient at 532 nm (a), volume depolarization ratio (b), color ratio (c) measured by National Institute for Environment Studies and aerosol optical depth (red), coarse mode fraction (blue) (d) measured by sun-photometer on 19 March 2010. The unit of Figure 3a is $10^{-2}$/km/sr.

effective receiver aperture; $\beta(z)$ is the backscattering cross sections of the aerosols and molecules at slant range $z$; and $T(z) = \exp\left[-\int_0^z \sigma(z)\mathrm{d}z\right]$ =the transmittance of the aerosols and molecules at slant range $z$, where $\sigma$ represents the extinction cross sections of the aerosols and molecules at range $z$, $\beta(z)$ is defined as the backscatter coefficient, and $\beta(z) \cdot T^2(z)$ is defined as the attenuated backscatter coefficient.

The VDR is defined as the perpendicular components of ABC at 532 nm divided by the parallel components of the same coefficient. The expression is as follows:

$$\delta(r) = \beta_{532,\perp}(r)/\beta_{532,\parallel}(r) \quad (1)$$

where $\beta_{532,\perp}(r)$ and $\beta_{532,\parallel}(r)$ are the attenuated backscatter coefficients at the perpendicular and parallel channel at height $r$ above the ground. The sphericity of a particle is represented by its VDR, such that a value near 0 indicates a nearly spherical particle, while a large value indicates a nonspherical particle. The VDR of ice crystals is typically in the range of 30%–50% and depends on the crystal shape and aspect ratio. Lower values can be seen when horizontally oriented particles are present (Sassen & Benson, 2001). In contrast, the backscattering from spherical water droplets preserves the polarization of the incident light; therefore, the value of the VDR is close to 0. Ansmann et al. (2003) suggested that the VDR is predominantly influenced by the sphericity of the dust particles. Therefore, the polarization is sensitive to nonspherical particles, such as ice and dust particles. In a large number of previous publications, VDR acted as criteria to distinguish clouds, cloud phases, aerosols and aerosol types. Huang et al. (2015) and Liu et al. (2005) used VDR to differentiate pure dust and polluted dust.

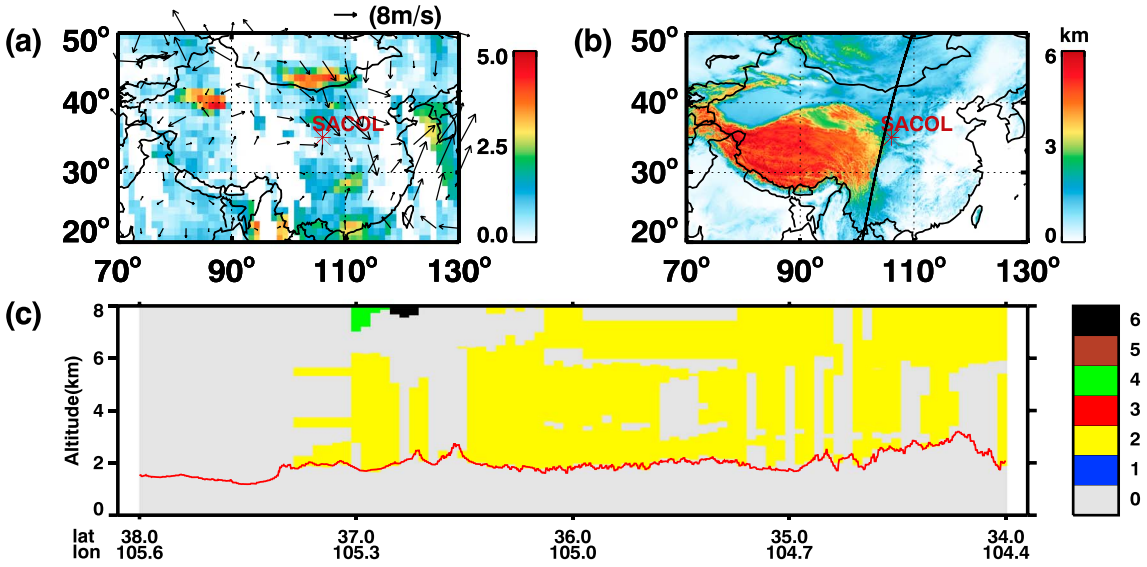


**Figure 5.** Distribution of aerosol index (color), wind speed (arrows) at 10 m from ECMWF (European Centre for Medium-Range Weather Forecasts) (a), overpass of Cloud-Aerosol Lidar and Infrared Pathfinder Satellite Observation (CALIPSO) (b) and vertical feature mask from CALIPSO (c) on 19March 2010.The colors in Figure 4b represent topographical elevation. In Figure 4c, 1 = marine, 2 = dust, 3 = polluted continental, 4 = clean continental, 5 = polluted dust, and 6 = smoke. SACOL = Semi-Arid Climate and Environment Observatory of Lanzhou University.

The CR is defined as the ratio of the ABC at 1064 nm to that at 532 nm. The expression is as follows:

$$x(r) = \beta_{1064}(r)/\beta_{532}(r) \tag{2}$$

where $\beta_{1064}(r)$ *and* $\beta_{532}(r)$ is the attenuated backscatter coefficients measured at 1,064 and 532 nm at height $z$ above the ground. The CR is an indicator of the particle size as well as particle's variable scattering of light across the available spectra. A large value of CR indicates a large particle and vice versa. The CR can be used to distinguish clouds and aerosols. In addition, CR is sensitive to the orientation, shape, and size of the particle.

When the lidar signal is processed, the general rules used in classifications are as follows: ABC values at 532 nm were located within the ranges of 0.08–0.16 $10^{-2}$/km/sr, 0.16–0.44 × $10^{-2}$/km/sr and 0.44–0.72 × $10^{-2}$/km/sr, corresponding to low, medium, and high aerosol concentrations, respectively (Lüthi et al., 2015). If the VDR is high (~0.17), then the layer is dominated by dust; if the VDR is low (~0.02) and the CR is high (~0.35), then the layer is dominated by pollutants; and if the VDR is somewhere in the middle and the CR is high, then the layer should be a mixture of dust and pollutants (and possibly other types of aerosols; Liu et al., 2008). Therefore, in this study, ABC values located within the range of 0.08–0.72 $10^{-2}$/km/sr, VDR values located within the range of 0.1–0.5 and CR values smaller than 2.0 were used to identify dust aerosols.

### 3.2. Dust Detection Using Sun Photometer Data

The criteria for the identification of pure and polluted dust were proposed by Bi et al. (2017). (1) Particles with high aerosol optical depth at 440 nm ($AOD_{440} \geq 0.4$) and a low Angstrom wavelength exponent ($\alpha < 0.2$) at 440–870 nm are defined as pure dust that maintains high accuracy of pure Asian dust and eliminates most fine-mode aerosols. (2) The particles with $AOD_{440} \geq 0.4$ and $0.2 < \alpha < 0.6$ are classified as polluted dust, which is mainly dominated by dust and might mix with other anthropogenic aerosols. Pure dust and polluted dust aerosols were identified only when the two criteria above were satisfied.

## 4. Case Studies

### 4.1. Pure Dust Case

Lidar signals dependent on height and time were used to distinguish dust from cloud droplets and air molecules. The values of ABC and CR for dust are smaller than those of clouds and greater than those of air

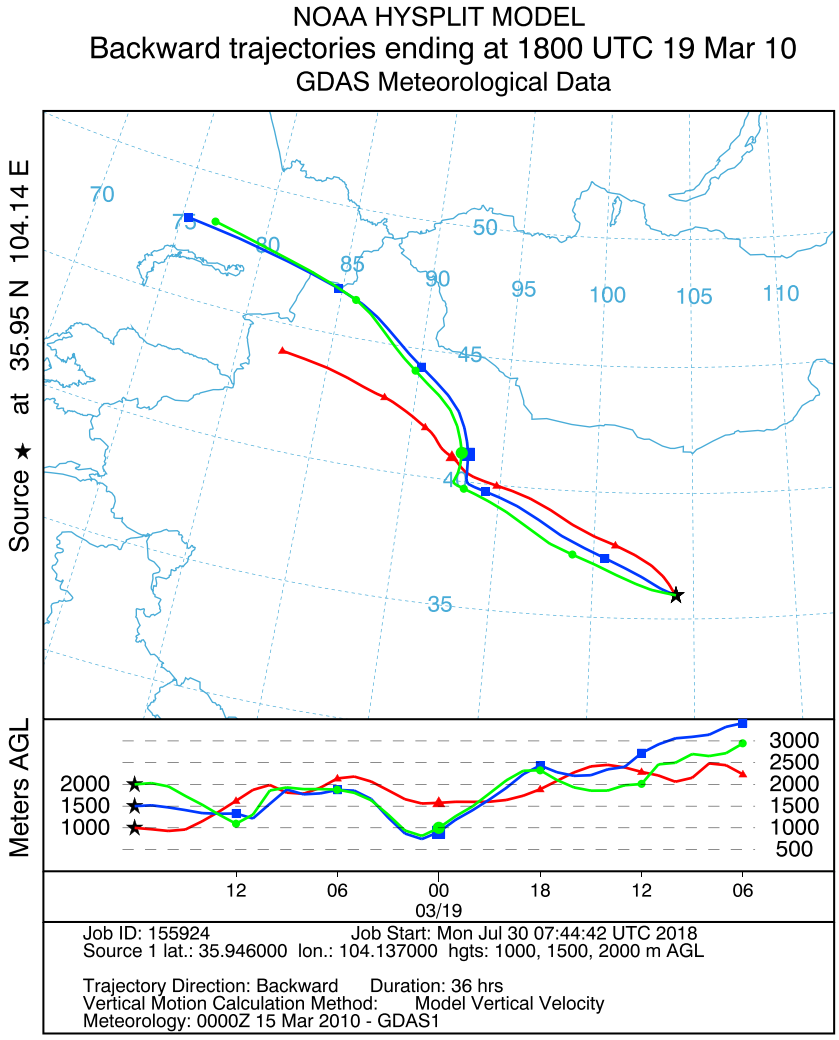


**Figure 6.** Thirty-six-hour back trajectories of air parcels passing through Semi-Arid Climate and Environment Observatory of Lanzhou University (SACOL) on 19 March 2010 by using the National Oceanic and Atmospheric Administration (NOAA) fourth-generation Hybrid Single-Particle Lagrangian Integrated Trajectory (HYSPLIT) model. GDAS = Global Data Assimilation System.

molecules. Figures 4a–4c presents the dust case observed by the NIES lidar on 19 March 2010. Generally, the NIES lidar products indicate aerosols with green-yellow-orange color schemes and clouds with white-gray color schemes. As shown in Figure 4, there was an aerosol layer from the surface up to 2 km with ABC, VDR, and CR values located within the ranges of 0.25–0.72 $\times$ $10^{-2}$/km/sr, 0.2–0.4, and 0.6–1.0, respectively. AOD was approximately 0.8–1.0, and the coarse mode fraction was over 0.8. Surface weather records showed that there was floating dust on that day. Therefore, this aerosol layer detected at SACOL could be regarded as a pure dust layer.

AI was over 2.5 in Mongolia and the Taklamakan region, which suggested the occurrence of a dust storm (as shown in Figure 5a). Dust aerosols were transported to SACOL as a result of the northwest wind, and dust aerosols within 6 km above the ground were detected in the west of SACOL by the CALIPSO observation (as shown in Figure 5c). The back trajectories from the HYSPLIT model were used to investigate the origins and transport of the dust aerosols as shown in Figure 6.The back trajectory started at SACOL which is marked with a black star. The trajectories are marked with different colors indicating starting points at different altitudes, and the altitudes of the air-entrained dust particles during their transport are provided at the bottom of Figure 6. It was clear that the dust aerosols detected at SACOL originated from the neighboring Gobi Desert in Mongolia and were transported to SACOL with a northwest wind.

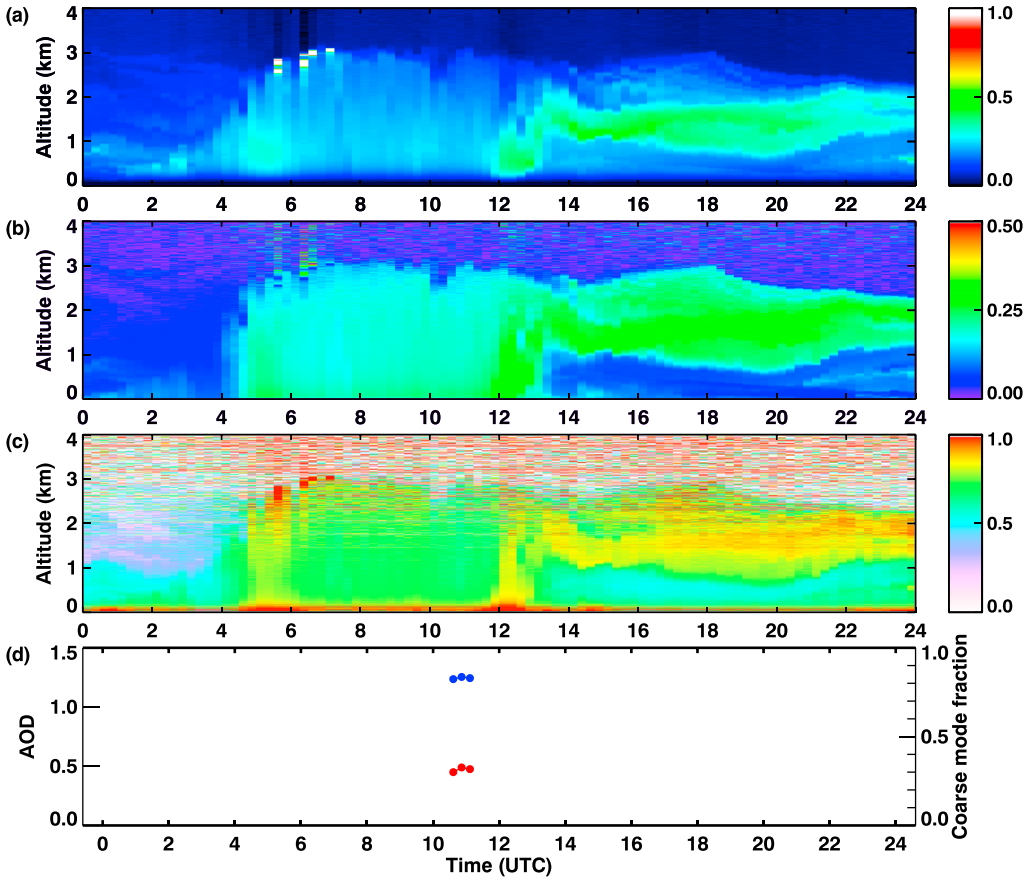


**Figure 7.** Same as Figure 3 but for 29 July 2010.

### 4.2. Polluted Dust Case

Figures 7a–7c shows a polluted dust case observed by the NIES lidar on 29 July 2010. There was an aerosol layer from the surface up to 3 km with ABC, VDR and CR located within the ranges of 0.15–0.6 $\times 10^{-2}$/km/sr, 0.06–0.3, and 0.5–0.8, respectively. AOD was approximately 0.5, and the coarse mode fraction was approximately 0.85. Surface weather record showed that there was no dust event on that day. In the Taklamakan region, the average value of AI wasapproximately1.5, which suggested there was a weak dust event (as shown in Figure 8a). Near the SACOL, polluted dust and smoke aerosols were detected from the surface to 2 km above the ground in the daytime, and dust aerosols were detected up to 1 km above the ground in the nighttime by the CALIPSO observation (as shown in Figures 8b–8d). Dust aerosols were transported to SACOL by the northwest wind, and polluted dust and smoke aerosols were transported to SACOL by the south wind.

The back trajectories from the HYSPLIT model (as shown in Figure 9) were used to study the source and transport of the dust aerosols. The dust aerosols detected at SACOL originated from the neighboring Taklamakan Desert. There were two main pathways: the northern pathway, by which pure dust aerosols were transported to SACOL, and the southern pathway, by which polluted dust and smoke aerosols were transported to SACOL. When dusts arrived at SACOL, the pure dust, polluted dust and smoke aerosols mixed together.

About the potential uncertainties in the meteorology/trajectory, four types of uncertainties have been summarized in Ma et al. (2015). The first type is the observation measurements uncertainty in the meteorology. The second is the prediction uncertainty caused by model. The third is physical uncertainty caused by the spatial and temporal disagreement. The last is the computation uncertainty including integral uncertainty

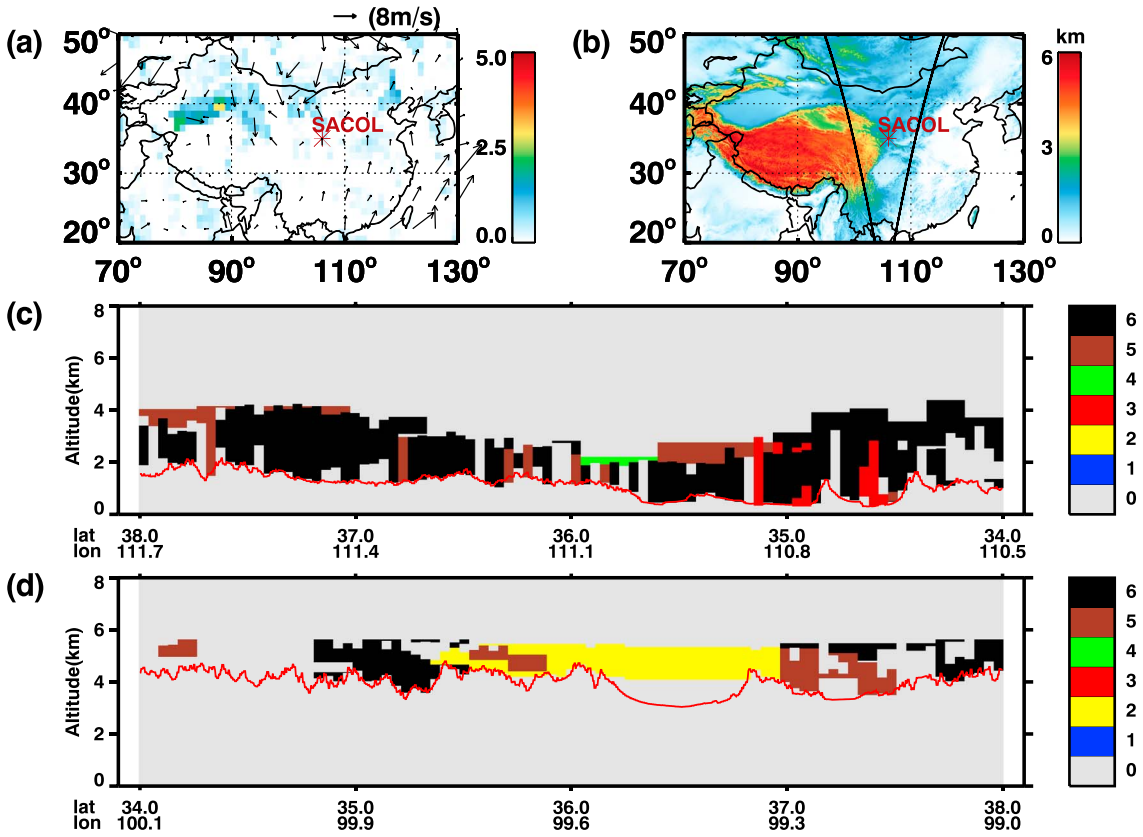


**Figure 8.** Distribution of aerosol index (color), wind speed (arrows) at 10 m from ECMWF (a), overpass of CALIPSO (b) and vertical feature mask at nighttime (c) and daytime (d) from CALIPSO on 29July 2010.The colors in Figure 7b represent topographical elevation. In Figures 7c and 7d, 1 = marine, 2 = dust, 3 = polluted continental, 4 = clean continental, 5 = polluted dust, 6 = smoke. SACOL = Semi-Arid Climate and Environment Observatory of Lanzhou University; ECMWF = European Centre for Medium-Range Weather Forecasts; CALIPSO = Cloud-Aerosol Lidar and Infrared Pathfinder Satellite Observation.

and resolution uncertainty. Using the HYSPLIT backward trajectory model, the 3-day forward trajectory of the 100 m air particle at the Hetian station at 12 o'clock on 12 March 2010 was simulated, and the integral error and resolution error in the trajectory calculation were analyzed. In the simulation test, the integral error has little contribution to the calculation error of the trajectory. With the extension of the integration time, the integral error increases slightly. The resolution error is different at different integral moments and is related to the terrain height and the weather system. In the trajectory mode, the trajectory calculation is based on the linear interpolation of wind speed in time and space. Therefore, the uncertainty of trajectory simulation is also related to interpolation. It has a significant influence on the calculation results of the trajectory when using driving data of different resolutions. The contribution of the resolution error to the trajectory calculation error is much larger than the integral error caused by the truncation approximation in the integration process.

## 5. Comparison of the Optical Properties of Two Types of Dust

A histogram of the AOD, AC, VDR, and CR for both pure dust and polluted dust is shown in Figures 10a–10d. The number of cases of pure dust and polluted dust aerosol was approximately 320 and 600, respectively. Using these frequency distributions, we can constrain satellite observation and model results. The AOD of pure dust was widely distributed within the range of 0.4–1.1, while 80% of the AOD values for polluted dust were smaller than 0.6. The mean value of VDR for pure dust was greater than that for polluted dust, which means that polluted dust was more spherical. The peak value of VDR for pure dust and polluted dust was 0.21 and 0.31, respectively. Freudenthaler et al. (2009) and Wandinger et al. (2010) both found that the particle depolarization ratio of pure dust aerosol was

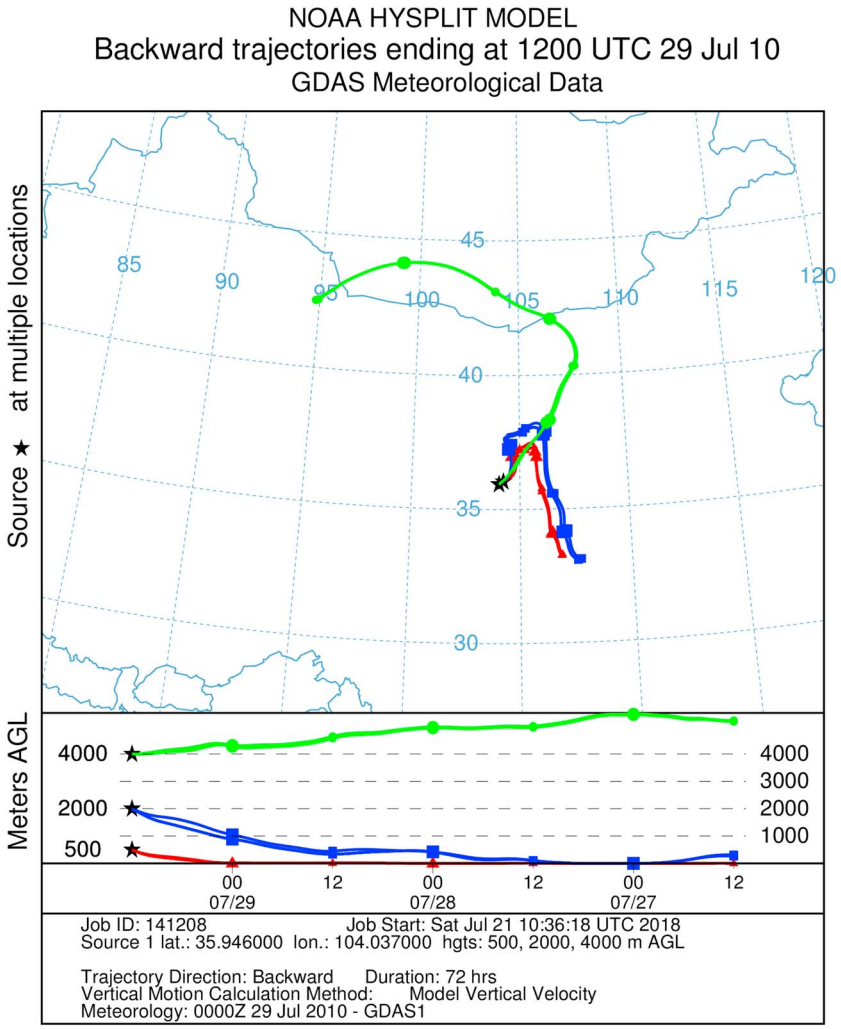


**Figure 9.** Seventy-two-hour back trajectories of air parcels passing through Semi-Arid Climate and Environment Observatory of Lanzhou University on 29 July 2010 by using the National Oceanic and Atmospheric Administration (NOAA) fourth-generation Hybrid Single-Particle Lagrangian Integrated Trajectory (HYSPLIT) model. GDAS = Global Data Assimilation System.

approximately 0.3 during SAMUM-1 (Saharan Mineral Dust Experiment) and SAMUM-2.The frequency distribution of CR showed that mean value of pure dust was larger than that of polluted dust. When the CR was larger than 0.8, it was mostly pure dust. In the source regions, the CR values of dust particles were between 0.7 and 1.0 (He & Yi, 2015; Huang et al., 2007).

The polluted dust aerosol was more spherical; therefore, VDR could be used to discriminate pure dust and polluted dust. The threshold value of 0.25 was proposed, which was consistent with Huang et al. (2015). Using this simple classification method, the misclassification for pure dust and polluted dust was 20.7% and 18.6%, respectively. Meanwhile, the total misclassification remained at a low level. Although most of the pure dust and polluted dust could be classified using the VDR threshold, the overlapping value between 0.24 and 0.26 may indicate ambiguous values for distinguishing pure dust and polluted dust via the VDR approach alone. Extra effort is still needed to reduce the misclassification. The reason why we could use VDR to discriminate pure dust and polluted dust aerosol is that dust mixes with smoke or other anthropogenic aerosols during transport, which makes the mixed aerosol nearly spherical. For example, dust particles can be fully mixed with inorganic salt (Fan et al., 1996; Shen et al., 2007; Sun et al., 2005); pollution elements such as Se, Ni, Pb, Br, Cu (Zhang et al., 2005); black carbon (Kim

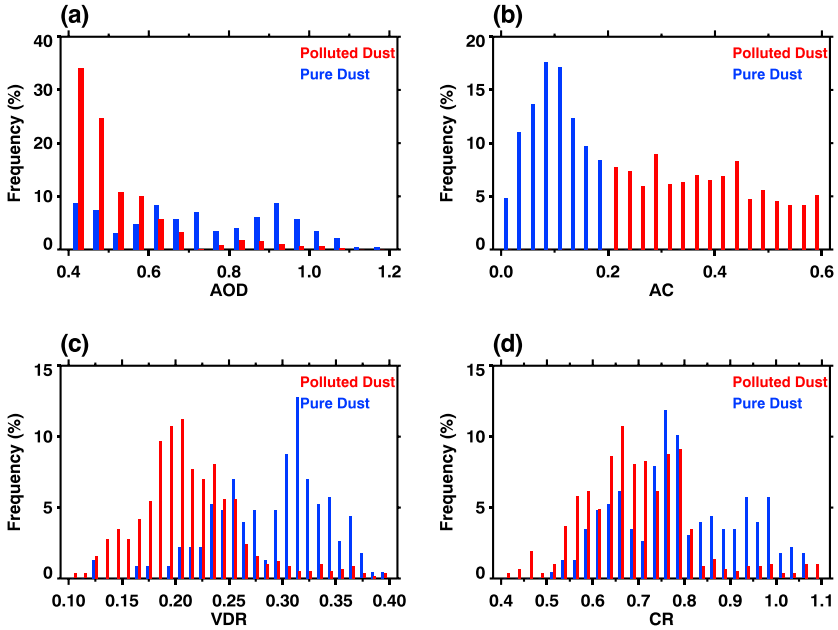


**Figure 10.** Comparison of the frequency distributions of aerosol optical depth (AOD) (a), AC (b), volume depolarization ratio (VDR) (c), and color ratio (CR) (d) for pure dust (blue) and polluted dust (red).

et al., 2004); VOCs; (volatile organic compounds) and polyaromatic hydrocarbon during long-range transport (He & Yi, 2015).

The relationship between the layer-integrated ABC and the layer-integrated VDR was used to distinguish dust aerosols, water clouds, and ice clouds, and the obviously different distributions of these molecules can be used to identify these features (Zhou, Huang, Huang, Li, et al., 2013). A scatterplot of the particle depolarization ratio at 532 nm and the backscattering CR was used to separate the clusters of spherical air-pollution aerosols and Asian dust (Sugimoto et al., 2002). Here we also attempted to investigate the relationship between the VDR and the CR for pure dust and polluted dust aerosols. Figure 11 shows the percentage of occurrences of pure dust and polluted dust in a 0.01 × 0.01 pixel. The distribution of VDR and CR for pure dust aerosols was wider than that for polluted dust. The relationship between VDR and CR showed that the VDR was located within the ranges of 0.2–0.42 and 0.15–0.26 for pure dust aerosol and polluted dust aerosol, and the CR was located within the ranges of 0.5–1.1 and 0.5–0.8, respectively. Additionally, a positive correlation between VDR and CR was observed, which was consistent with Freudenthaler et al. (2009).

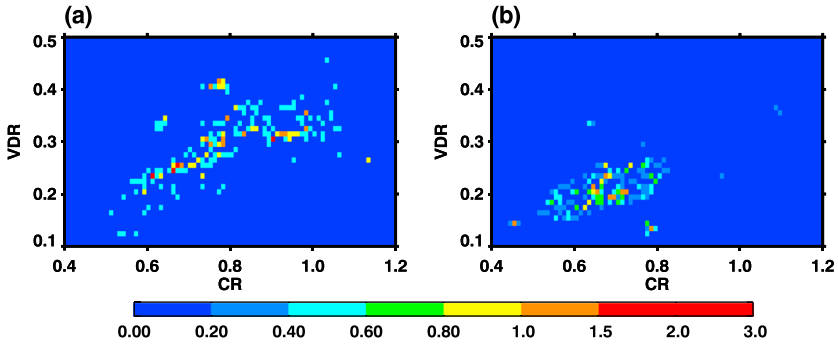


**Figure 11.** Relationship between attenuated backscattering coefficient and volume depolarization ratio for (a) pure dust and (b) polluted dust. The colors represent the percentage in each 0.01*0.01 box.

## 6. Conclusion and Discussion

Pure dust and polluted dust could be distinguished by using a combination of ground-based L2S-SM-II dual-band polarization lidar data, sun photometer data, surface weather station data, and back trajectories from the HYSPLIT model. The optical properties of pure dust and polluted dust were studied. The conclusions are as follows.

The frequency distribution of VDR value showed that the mean value of pure dust was greater than that of polluted dust with peak values of 0.31 and 0.21, respectively. The frequency distribution of CR showed that the mean value of pure dust was greater than that of polluted dust, and pure dust was dominant when color ratio was larger than 0.8.

The relationship between VDR and CR showed that the distribution of pure dust was wider than that of polluted dust. The VDR of pure dust and polluted dust was located within the ranges of 0.2–0.42 and 0.15–0.26, and the CR was located within the ranges of 0.5–1.1 and 0.5–0.8, respectively. Additionally, a positive correlation between VDR and CR was observed in both types of dust aerosols.

Because the polluted dust aerosol was relatively spherical, VDR could be used to simply discriminate pure dust and polluted dust. Using the frequency distribution of VDR, the threshold value of 0.25 was proposed to differentiate pure dust from polluted dust. The rate of misclassification was 20.7% and 18.6% for pure dust and polluted dust, respectively. The overlapping value between 0.24 and 0.26 may indicate ambiguous values for distinguishing pure dust and polluted dust via the VDR approach alone. Additional effort is needed to reduce the misclassification.

To investigate the mixing of Asian dusts with anthropogenic aerosols during their long-range transports, an intensive spring aerosol in situ sampling campaign was conducted over northwestern and northern China as well as Shanghai in eastern China during the spring of 2007 (K. Huang et al., 2010). The origins of dusts and mixing mechanisms were studied by using the aerosol concentrations measured in this campaign. The dust from the Taklimakan Desert was rarely polluted, which was similar to the pure dust in our study. The dust from high-calcium Mongolia Gobi Desert had a considerable chemical reactivity and was mixed with sulfur precursors emitted from coal mines on the pathway of the long-range transport, which was similar to the polluted dust in our study.

Aerosol optical properties were continuously measured with the NIES compact Raman lidar in Beijing, China, from 15 to 31 December 2007 (Xie et al., 2008). The results indicated that the VDR was mostly below 10% during the pollution episode, whereas it was greater than 20% during the Asian dust episode. The average VDR of the nonspherical mineral dust particles was $19.54 \pm 0.53\%$, which is slightly smaller than that in our results. The particle depolarization ratio (PDR) is a useful indicator of nonsphericity for the identification of ice clouds (Sassen, 1991) and dust layers (Kobayashi et al., 1985; Murayama et al., 1999). PDR could be derived from the observed total to Rayleigh backscatter ratio and VDR. Shimizu et al. (2004) found that in Beijing, the PDR distribution centered on 0.15–0.2 with a broad range, and there was no peak below 0.1. This broad distribution showed that the air always contained both nonspherical (dust particles) and spherical particles. PDR will be used to detect pure dust and polluted dust in our future work.

The mixing state of polluted dust has been studied by using chemical methods (e.g., Song et al., 2013; Sullivan et al., 2007). Additionally, internally mixed Asian dust with air-pollution aerosols was detected by analyzing the scatter diagram between the depolarization ratio from the NIES lidar and the forward scattering intensity from the POPC (Sugimoto, Nishizawa, Shimizu, Matsui, Kobayashi, et al., 2015). The results showed that the backscattering CR of the polluted dust was comparable to that of pure dust, but the depolarization ratio was lower for polluted dust. However, it is difficult to study the mixing state of polluted dust by using NIES lidar data alone.

**Acknowledgments**
The meteorological data used are archived in the China Meteorological Data Network from China Meteorological Administration Meteorological Data Center (http://www.cma.gov.cn/2011qxfw/2011qsjgx/), and lidar data are archived in the sharing data of SACOL (http://climate.lzu.edu.cn/data/index.asp). This work is supported by the National Fund Committee Innovation Group (grant 41521004), General Program (grant 41775021), National Natural Science Foundation of China (grant 41305026), and the National Natural Science Foundation of China (grant 41375032). Ground-based lidar data were obtained from the Semi-Arid Climate and Environment Observatory of Lanzhou University (SACOL). The surface station weather data were obtained from the China Meteorological Data Sharing Service System.

## References

Ansmann, A., Bösenberg, J., Chaikovsky, A., Comerón, A., Eckhardt, S., Eixmann, R., et al. (2003). Long-range transport of Saharan dust to northern Europe: The 11–16 October 2001 outbreak observed with EARLINET. *Journal of Geophysical Research*, *108*(D24), 4783. https://doi.org/10.1029/2003JD003757

Bi, J., Huang, J., Shi, J., Hu, Z., Zhou, T., Zhang, G., et al. (2017). Measurement of scattering and absorption properties of dust aerosol in a Gobi farmland region of northwestern China—A potential anthropogenic influence. *Atmospheric Chemistry and Physics*, *17*, 1–41.

Chen, B., Huang, J., Minnis, P., Hu, Y., Yi, Y., Liu, Z., et al. (2010). Detection of dust aerosol by combining CALIPSO active lidar and passive IIR measurements. *Atmospheric Chemistry and Physics*, *10*(2), 3423–3456. https://doi.org/10.5194/acpd-10-3423-2010

Chen, S., Huang, J., Qian, Y., Zhao, C., Kang, L., Yang, B., et al. (2017). An overview of mineral dust modeling over East Asia. *Journal of Meteorological Research*, *31*(4), 633–653. https://doi.org/10.1007/s13351-017-6142-2

Chen, S., Jiang, N., Huang, J., Xu, X., Zhang, H., Zang, Z., et al. (2018). Quantifying contributions of natural and anthropogenic dust emission from different climatic regions. *Atmospheric Environment*, *191*(2018), 94–104. https://doi.org/10.1016/j.atmosenv.2018.07.043

Elterman, L. O. U. I. S. (1966). Aerosol measurements in the troposphere and stratosphere. *Applied Optics*, *5*(11), 1769–1776. https://doi.org/10.1364/AO.5.001769

Fan, X. B., Okada, K., Niimura, N., Kai, K., Arao, K., Shi, G. Y., et al. (1996). Mineral particles collected in China and Japan during the same Asian dust-storm event. *Atmospheric Environment*, *30*(2), 347–351. https://doi.org/10.1016/1352-2310(95)00271-Y

Fernald, F. G. (1984). Analysis of atmospheric lidar observations: Some comments. *Applied Optics*, *23*(5), 652–653. https://doi.org/10.1364/AO.23.000652

Freudenthaler, V., Esselborn, M., Wiegner, M., Heese, B., Tesche, M., Ansmann, A., et al. (2009). Depolarization ratio profiling at several wavelengths in pure Saharan dust during SAMUM 2006. *Tellus Series B: Chemical and Physical Meteorology*, *61*(1), 165–179. https://doi.org/10.1111/j.1600-0889.2008.00396.x

Garrett, T., & Zhao, C. (2013). Ground-based remote sensing of thin clouds in the Arctic. *Atmospheric Measurement Techniques*, *6*(5), 1227–1243. https://doi.org/10.5194/amt-6-1227-2013

Guan, X., Huang, J., Zhang, Y., Xie, Y., & Liu, J. (2016). The relationship between anthropogenic dust and population over global semi-arid regions. *Atmospheric Chemistry and Physics*, *16*(8), 5159–5169. https://doi.org/10.5194/acp-16-5159-2016

He, Y., & Yi, F. (2015). Dust aerosols detected using a ground-based polarization lidar and CALIPSO over Wuhan (30.5 N, 114.4 E), China. *Advances in Meteorology*, *2015*, 1–18. https://doi.org/10.1155/2015/536762

Hou, X., Zhuang, G., Sun, Y., & An, Z. (2006). Characteristics and sources of polycyclic aromatic hydrocarbons and fatty acids in $PM_{2.5}$ aerosols in dust season in China. *Atmospheric Environment*, *40*(18), 3251–3262. https://doi.org/10.1016/j.atmosenv.2006.02.003

Hua, D., & Kobayashi, T. (2005a). Ultraviolet Rayleigh–Mie lidar by use of a multicavityFabry–Perot filter for accurate temperature profiling of the troposphere. *Applied Optics*, *44*(30), 6474–6478. https://doi.org/10.1364/AO.44.006474

Hua, D., & Kobayashi, T. (2005b). UV Rayleigh–Mie Raman lidar for simultaneous measurement of atmospheric temperature and relative humidity profiles in the troposphere. *Japanese Journal of Applied Physics*, *44*(3), 1287–1291. https://doi.org/10.1143/JJAP.44.1287

Hua, D., Liu, J., Uchida, K., & Kobayashi, T. (2007). Daytime temperature profiling of planetary boundary layer with ultraviolet rotational Raman lidar. *Japanese Journal of Applied Physics*, *46*(9A), 5849–5852. https://doi.org/10.1143/JJAP.46.5849

Hua, D., Uchida, M., & Kobayashi, T. (2005a). Ultraviolet Rayleigh–Mie lidar for daytime-temperature profiling of the troposphere. *Applied Optics*, *44*(7), 1315–1322. https://doi.org/10.1364/AO.44.001315

Hua, D., Uchida, M., & Kobayashi, T. (2005b). Ultraviolet Rayleigh–Mie lidar with Mie-scattering correction by Fabry–Perot etalons for temperature profiling of the troposphere. *Applied Optics*, *44*(7), 1305–1314. https://doi.org/10.1364/AO.44.001305

Huang, J., Fu, Q., Su, J., Tang, Q., Minnis, P., Hu, Y., et al. (2009). Taklimakan dust aerosol radiative heating derived from CALIPSO observations using the Fu-Liou radiation model with CERES constraints. *Atmospheric Chemistry and Physics*, *9*(12), 4011–4021. https://doi.org/10.5194/acp-9-4011-2009

Huang, J., Ge, J., & Weng, F. (2007). Detection of Asia dust storms using multi-sensor satellite measurements. *Remote Sensing of Environment*, *110*(2), 186–191. https://doi.org/10.1016/j.rse.2007.02.022

Huang, J., Lin, B., Minnis, P., Wang, T., Wang, X., Hu, Y., et al. (2006). Satellite-based assessment of possible dust aerosols semi-direct effect on cloud water path over East Asia. *Geophysical Research Letters*, *33*, L19802. https://doi.org/10.1029/2006GL026561

Huang, J., Minnis, P., Lin, B., Wang, T., Yi, Y., Hu, Y., et al. (2006). Possible influences of Asian dust aerosols on cloud properties and radiative forcing observed from MODIS and CERES. *Geophysical Research Letters*, *33*, L06824. https://doi.org/10.1029/2005GL024724

Huang, J., Minnis, P., Lin, B., Yi, Y., Khaiyer, M. M., Arduini, R. F., et al. (2005). Advanced retrievals of multi-layered cloud properties using multi-spectral measurements. *Journal of Geophysical Research*, *110*, D15S18. https://doi.org/10.1029/2004JD005101

Huang, J., Minnis, P., Yan, H., Yi, Y., Chen, B., Zhang, L., & Ayers, J. K. (2010). Dust aerosol effect on semi-arid climate over Northwest China detected from A-Train satellite measurements. *Atmospheric Chemistry and Physics*, *10*(14), 6863–6872. https://doi.org/10.5194/acp-10-6863-2010

Huang, J., Wang, T., Wang, W., Li, Z., & Yan, H. (2014). Climate effects of dust aerosols over East Asian arid and semiarid regions. *Journal of Geophysical Research: Atmospheres*, *119*, 11,398–11,416. https://doi.org/10.1002/2014JD021796

Huang, J., Zhang, W., Zuo, J., Bi, J., Shi, J., Wang, X., et al. (2008). An overview of the semi-arid climate and environment research observatory over the loess plateau. *Advances in Atmospheric Sciences*, *25*(6), 906–921. https://doi.org/10.1007/s00376-008-0906-7

Huang, J. P., Liu, J. J., Chen, B., & Nasiri, S. L. (2015). Detection of anthropogenic dust using CALIPSO lidar measurements. *Atmospheric Chemistry and Physics*, *15*(20), 11,653–11,665. https://doi.org/10.5194/acp-15-11653-2015

Huang, K., Zhuang, G., Li, J., Wang, Q., Sun, Y., Lin, Y., & Fu, J. S. (2010). Mixing of Asian dust with pollution aerosol and the transformation of aerosol components during the dust storm over China in spring 2007. *Journal of Geophysical Research*, *115*, D00K13. https://doi.org/10.1029/2009JD013145

Kang, L., Chen, S., Huang, J., Zhao, S., Ma, X., Yuan, T., et al. (2017). The spatial and temporal distributions of absorbing aerosols over East Asia. *Remote Sensing*, *9*(10), 1050. https://doi.org/10.3390/rs9101050

Kim, K. W., He, Z., & Kim, Y. J. (2004). Physicochemical characteristics and radiative properties of Asian dust particles observed at Kwangju, Korea, during the 2001 ACE-Asia intensive observation period. *Journal of Geophysical Research*, *109*, D19S02. https://doi.org/10.1029/2003JD003693

Kobayashi, A., Hayashida, S., Okada, K., & Iwasaka, Y. (1985). Measurements of the polarization properties of Kosa (Asian dust-storm) particles by a laser radar in spring 1983. *Journal of the Meteorological Society of Japan. Ser. II*, *63*(1), 144–149.

Li, Z. (2004). Aerosols and climate: A perspective over East Asia. In Observation, theory and modeling of atmospheric variability: Selected papers of Nanjing Institute of Meteorology Alumni in Commemoration of Professor Jijia Zhang, 501–525. https://doi.org/10.1142/9789812791139_0025

Liu, J., Chen, B., & Huang, J. (2014). Discrimination and validation of clouds and dust aerosol layers over the Sahara desert with combined CALIOP and IIR measurements. *Journal of Meteorological Research*, *28*(2), 185–198. https://doi.org/10.1007/s13351-014-3051-5

Liu, Y., Huang, J., Shi, G., Takamura, T., Khatri, P., Bi, J., et al. (2011). Aerosol optical properties and radiative effect determined from sky-radiometer over Loess Plateau of Northwest China. *Atmospheric Chemistry and Physics*, *11*(22), 11,455–11,463. https://doi.org/10.5194/acp-11-11455-2011

Liu, Z., Liu, D., Huang, J., Vaughan, M., Uno, I., Sugimoto, N., et al. (2008). Airborne dust distributions over the Tibetan Plateau and surrounding areas derived from the first year of CALIPSO lidar observations. *Atmospheric Chemistry and Physics*, *8*(16), 5045–5060. https://doi.org/10.5194/acp-8-5045-2008

Liu, Z., Omar, A. H., Hu, Y., Vaughan, M. A., Winker, D. M., Poole, L. R., TA Kovacs (2005). CALIOP algorithm theoretical basis document. Part 3: Scene classification algorithms. NASA-CNES document PC-SCI-203.

Lüthi, Z. L., Skerlak, B., Kim, S. W., Lauer, A., Mues, A., Rupakheti, M., & Kang, S. (2015). Atmospheric brown clouds reach the Tibetan plateau by crossing the Himalayas. *Atmospheric Chemistry and Physics*, *15*(11), 6007–6021. https://doi.org/10.5194/acp-15-6007-2015

Ma, Y., Lu, H., & Liu, T. (2015). Trajectory calculation error assessment for HYSPLIT. *Journal of Nanjing University of Information Science & Technology*, *2015*(1), 86–91.

Murayama, T., Okamoto, H., Kaneyasu, N., Kamataki, H., & Miura, K. (1999). Application of lidar depolarization measurement in the atmospheric boundary layer: Effects of dust and sea-salt particles. *Journal of Geophysical Research*, *104*, 31,781–31,792. https://doi.org/10.1029/1999JD900503

Sassen, K. (1991). The polarization lidar technique for cloud research: A review and current assessment. *Bulletin of the American Meteorological Society*, *72*(12), 1848–1866. https://doi.org/10.1175/1520-0477(1991)072<1848:TPLTFC>2.0.CO;2

Sassen, K. (2002). Indirect climate forcing over the western US from Asian dust storms. *Geophysical Research Letters*, *29*(10), 1465. https://doi.org/10.1029/2001GL014051

Sassen, K., & Benson, S. (2001). A mid-latitude cirrus cloud climatology from the Facility for Atmospheric Remote Sensing. Part II: Microphysical properties derived from lidar depolarization. *Journal of the Atmospheric Sciences*, *58*(15), 2103–2112. https://doi.org/10.1175/1520-0469(2001)058<2103:AMCCCF>2.0.CO;2

Shen, Z., Cao, J., Arimoto, R., Zhang, R., Jie, D., Liu, S., & Zhu, C. S. (2007). Chemical composition and source characterization of spring aerosol over Horqin sand land in northeastern China. *Journal of Geophysical Research*, *112*, D14315. https://doi.org/10.1029/2006JD007991

Shi, G., Wang, H., Wang, B., Li, W., Gong, S., Zhao, T., & Aoki, T. (2005). Sensitivity experiments on the effects of optical properties of dust aerosols on their radiative forcing under clear sky condition. *Journal of the Meteorological Society of Japan. Ser. II*, *83*, 333–346.

Shimizu, A., Sugimoto, N., Matsui, I., Arao, K., Uno, I., Murayama, T., et al. (2004). Continuous observations of Asian dust and other aerosols by polarization lidars in China and Japan during ACE-Asia. *Journal of Geophysical Research*, *109*, D19S17. https://doi.org/10.1029/2002JD003253

Sokolik, I. N., & Toon, O. B. (1996). Direct radiative forcing by anthropogenic airborne mineral aerosols. *Nature*, *381*(6584), 681–683. https://doi.org/10.1038/381681a0

Song, Y. C., Eom, H. J., Jung, H. J., Malek, M. A., Kim, H. K., Geng, H., & Ro, C. U. (2013). Investigation of aged Asian dust particles by the combined use of quantitative ED-EPMA and ATR-FTIR imaging. *Atmospheric Chemistry and Physics*, *13*(6), 3463–3480. https://doi.org/10.5194/acp-13-3463-2013

Su, J., Huang, J., Fu, Q., Minnis, P., Ge, J., & Bi, J. (2008). Estimation of Asian dust aerosol effect on cloud radiation forcing using Fu-Liouradiative model and CERES measurements. *Atmospheric Chemistry and Physics*, *8*(10), 2763–2771.

Sugimoto, N., Matsui, I., Shimizu, A., Uno, I., Asai, K., Endoh, T., & Nakajima, T. (2002). Observation of dust and anthropogenic aerosol plumes in the northwest Pacific with a two-wavelength polarization lidar on board the research vessel Mirai. *Geophysical Research Letters*, *29*(19), 1901. https://doi.org/10.1029/2002GL015112

Sugimoto, N., Nishizawa, T., Shimizu, A., Matsui, I., Jin, Y., Higurashi, A., et al. (2015). Continuous observation of atmospheric aerosols across East Asia. SPIE Newsroom, Oct, 21. https://doi.org/10.1117/2.1201510.006178

Sugimoto, N., Nishizawa, T., Shimizu, A., Matsui, I., & Kobayashi, H. (2015). Detection of internally mixed Asian dust with air pollution aerosols using a polarization optical particle counter and a polarization-sensitive two-wavelength lidar. *Journal of Quantitative Spectroscopy and Radiative Transfer*, *150*, 107–113. https://doi.org/10.1016/j.jqsrt.2014.08.003

Sullivan, R. C., Guazzotti, S. A., Sodeman, D. A., & Prather, K. A. (2007). Direct observations of the atmospheric processing of Asian mineral dust. *Atmospheric Chemistry and Physics*, *7*(5), 1213–1236. https://doi.org/10.5194/acp-7-1213-2007

Sun, Y., Zhuang, G., Wang, Y., Zhao, X., Li, J., Wang, Z., & An, Z. (2005). Chemical composition of dust storms in Beijing and implications for the mixing of mineral aerosol with pollution aerosol on the pathway. *Journal of Geophysical Research*, *110*, D24209. https://doi.org/10.1029/2005JD006054

Tegen, I., & Fung, I. (1995). Contribution to the atmospheric mineral aerosol load from land surface modification. *Journal of Geophysical Research*, *100*, 18,707–18,726. https://doi.org/10.1029/95JD02051

Twomey, S. A., Piepgrass, M., & Wolfe, T. L. (1984). An assessment of the impact of pollution on global cloud albedo. *Tellus B*, *36*(5), 356–366. https://doi.org/10.3402/tellusb.v36i5.14916

Wandinger, U., Tesche, M., Seifert, P., Ansmann, A., Müller, D., & Althausen, D. (2010). Size matters: Influence of multiple scattering on CALIPSO light-extinction profiling in desert dust. *Geophysical Research Letters*, *37*, L10801. https://doi.org/10.1029/2010GL042815

Wang, Y., Zhao, C., Dong, Z., Li, Z., Hu, S., Chen, T., et al. (2018). Improved retrieval of cloud base heights from ceilometer using a non-standard instrument method. *Atmospheric Research*, *202*, 148–155. https://doi.org/10.1016/j.atmosres.2017.11.021

Xie, C., Nishizawa, T., Sugimoto, N., Matsui, I., & Wang, Z. (2008). Characteristics of aerosol optical properties in pollution and Asian dust episodes over Beijing, China. *Applied Optics*, *47*(27), 4945–4951. https://doi.org/10.1364/AO.47.004945

Xie, S., Liu, X., Zhao, C., & Zhang, Y. (2013). Sensitivity of CAM5 simulated Arctic clouds and radiation to ice nucleation parameterization. *Journal of Climate*, *26*(16), 5981–5999. https://doi.org/10.1175/JCLI-D-12-00517.1

Zhang, R., Arimoto, R., An, J., Yabuki, S., & Sun, J. (2005). Ground observations of a strong dust storm in Beijing in March 2002. *Journal of Geophysical Research*, *110*, D18S06. https://doi.org/10.1029/2004JD004589

Zhao, C., Liu, L., Wang, Q., Qiu, Y., Wang, W., Wang, Y., & Fan, T. (2016). Toward understanding the properties of high ice clouds at the Naqu site on the Tibetan plateau using ground-based active remote sensing measurements obtained during a short period in July 2014. *Journal of Applied Meteorology and Climatology*, *55*(11), 2493–2507. https://doi.org/10.1175/JAMC-D-16-0038.1

Zhao, C., Wang, Y., Wang, Q., Li, Z., Wang, Z., & Liu, D. (2014). A new cloud and aerosol layer detection method based on micropulselidar measurements. *Journal of Geophysical Research: Atmospheres*, *119*, 6788–6802. https://doi.org/10.1002/2014JD021760

Zhao, C., Xie, S., Klein, S. A., Protat, A., Shupe, M. D., Mcfarlane, S. A., et al. (2012). Toward understanding of differences in current cloud retrievals of ARM ground-based measurements. *Journal of Geophysical Research*, *117*, D10206. https://doi.org/10.1029/2011JD016792

Zhou, T., Huang, J., Huang, Z., Liu, J., Wang, W., & Lin, L. (2013). The depolarization–attenuated backscatter relationship for dust plumes. *Optics Express*, *21*(13), 15,195–15,204. https://doi.org/10.1364/OE.21.015195

Zhou, T., Huang, Z., Huang, J., Li, J., Bi, J., & Zhang, W. (2013). Study of vertical distribution of cloud over Loess Plateau based on a ground-based lidar system. *Journal of Arid Meteorology*, *2*, 004.